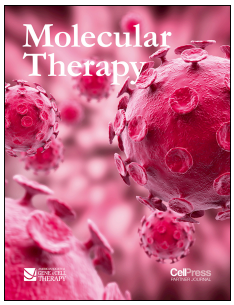

Type-1 Interferon Responses Underlie Tumor-Selective Replication of Oncolytic Measles Virus

Sarah Aref, Anna Z. Castleton, Katharine Bailey, Richard Burt, Aditi Dey, Daniel Leongamornlert, Rachel J. Mitchell, Dina Okasha, Adele K. Fielding

PII: S1525-0016(20)30086-1

DOI: https://doi.org/10.1016/j.ymthe.2020.01.027

Reference: YMTHE 5093

To appear in: *Molecular Therapy*

Received Date: 18 August 2019

Accepted Date: 31 January 2020

Please cite this article as: Aref S, Castleton AZ, Bailey K, Burt R, Dey A, Leongamornlert D, Mitchell RJ, Okasha D, Fielding AK, Type-1 Interferon Responses Underlie Tumor-Selective Replication of Oncolytic Measles Virus, *Molecular Therapy* (2020), doi: https://doi.org/10.1016/j.ymthe.2020.01.027.

Type-1 Interferon Responses Underlie Tumor-Selective Replication of Oncolytic Measles Virus

Sarah Aref[1], Anna Z. Castleton[1,3], Katharine Bailey[1], Richard Burt[1], Aditi Dey[1], Daniel Leongamornlert[2], Rachel J. Mitchell[1], Dina Okasha[1,4], Adele K. Fielding[1]

[1] UCL Cancer Institute, London, WC1E 6DD, UK

[2] Wellcome Trust Sanger Institute, Hinxton, Cambridgeshire, CB10 1SA, UK

[3] Current address: The Christie NHS Foundation Trust, Manchester, M20 4BX, UK

[4] Current address: Alexandria University Faculty of Medicine, Alexandria, Egypt

Corresponding author: Adele K. Fielding, UCL Cancer Institute, Paul O'Gorman Building, 72 Huntley St., London WC1E 6DD, UK.

email a.fielding@ucl.ac.uk

Conflict of interest: The authors have declared that no conflict of interest exists.

Short title:

High basal ISG levels restrict MV oncolysis

Summary

In this paper, we have investigated the mechanisms underlying tumour selectivity of oncolytic measles virus using a previously well-characterized model of sequential transformation of human bone marrow-derived mesenchymal stromal cells (BM-MSCs). We have demonstrated the contribution of the type 1 IFN pathway in resistance to MV infection as well as shown that the interferon-stimulated gene, *IFITM1*, acts as a restriction factor for oncolytic strains of MV.

Abstract

The mechanism of tumor selective replication of oncolytic measles virus (MV) is poorly understood. Using a step-wise model of cellular transformation, in which oncogenic hits were additively expressed in human bone marrow-derived mesenchymal stromal cells, we show that MV-induced oncolysis increased progressively with transformation. Type-1 interferon response to MV infection was significantly reduced and delayed, in accordance with the level of transformation. Consistently, we observed delayed and reduced STAT1 phosphorylation in the fully transformed cells. Pre-treatment with IFNβ restored resistance to MV-mediated oncolysis. Gene expression profiling to identify the genetic correlates of susceptibility to MV oncolysis revealed a dampened basal level of immune-related genes in the fully transformed cells compared to their normal counterparts. Interferon-induced transmembrane protein 1 (*IFITM1)* was the foremost basally downregulated immune gene. Stable *IFITM1* overexpression in MV-susceptible cells resulted in a 50% increase in cell viability and a significant reduction in viral replication at 24 hours post MV infection. Overall, our data indicate that the basal reduction in functions of the type 1 IFN pathway is a major contributor to the oncolytic selectivity of MV. In particular, we have identified *IFITM1* as a restriction factor for oncolytic MV, acting at early stages of infection.

Keywords Innate immune response, type 1 interferon, Measles virus (MV), interferon-induced transmembrane protein 1 (IFITM1), interferon stimulated gene (ISG)

Introduction

Over the last two decades, oncolytic viruses (OVs) have emerged as promising cancer therapeutics by preferentially infecting tumor cells, thereby mediating cell killing and eliciting an anti-tumor immune response.[1] Recombinant derivatives of the MV Edmonston-B vaccine strain (MV-Edm) are efficacious against a number of human malignancies[2] and are currently being evaluated in phase I/II clinical trials for the treatment of glioblastoma (NCT00450814), ovarian cancer (NCT02364713), breast cancer (NCT01846091), mesothelioma (NCT01503177), multiple myeloma (NCT01503177), head and neck cancer (NCT01846091) and malignant peripheral nerve sheath tumors (NCT02700230).

MV is an enveloped morbillivirus from the Paramyxoviruses family. It has a non-segmented negative single-stranded RNA genome encoding eight viral proteins, of which two envelope glycoproteins haemagglutinin (H) and fusion (F) proteins mediate attachment and entry into infected host cells, respectively.[3] Cellular entry of MV is facilitated by three known receptors; CD46[4, 5] SLAM[6] and nectin-4[7, 8] ;CD46 being the preferential receptor for vaccine strains. Upon infection, MV induces a strong cytopathic effect, which results in multi-nucleated syncytia.[3, 9]

The mechanism underlying the tumor selectivity of oncolytic MV is unclear. The selective tropism of oncolytic MV has been attributed to CD46 overexpression by tumor cells.[10] However, SLAM-dependent entry of oncolytic MV has been documented in mantle cell lymphoma cells and xenografts, which was not correlated to CD46 expression levels.[11] Defective type 1 interferon signalling, first shown by

Stojdl *et al.,* (2000) to facilitate oncolytic vesicular stomatitis virus replication also represents a potential mechanism of action for oncolytic MV.[12] In normal cells, sensing of MV RNA by pathogen recognition receptors RIG-I and MDA-5 results in the production of type 1 interferon (IFNα/β).[13-15]. The binding of interferons to their cognate receptor (IFNAR) on infected and neighboring uninfected cells activates the JAK/STAT signaling pathway, resulting in the phosphorylation of STAT1 and STAT2. Phosphorylated STAT1 and STAT2 bind to IRF9 to form the ISGF3 transcription factor complex which then binds to IFN-stimulated response elements (ISREs) in promoters of interferon-stimulated genes (ISGs) to induce the transcription of hundreds of ISGs. These ISGs collectively establish an antiviral state in the infected cell by inhibiting multiple stages of viral infection.[16, 17] Indeed, constitutive interferon pathway activation was identified as the key determinant for MV replication in MV-permissive and -resistant glioblastoma xenografts.[18]

We set out to probe the precise mechanisms of oncolytic MV specificity using an established step-wise model of cellular transformation, in which progressive oncogenic hits were stably and additively expressed in human bone marrow-derived mesenchymal stromal cells (MSCs).[19] We showed that progressive MV-mediated cell killing is closely correlated with the degree of transformation, and that lower basal expression of genes within the type 1 IFN pathway play an important role in facilitating MV infection. In particular, we implicate the ISG *IFITM1* in the tumor-selective replication and killing mediated by oncolytic MV.

Results

Susceptibility to MV-mediated oncolysis is positively correlated with progressive transformation of MSCs

To investigate MV replication kinetics in the model of progressively transformed human bone marrow-derived MSCs, cells at all the transformational stages, as shown in figure 1, were infected with MV-NSe at an MOI of 1.0. Figure 2a shows MV-specific cell death at 3 timepoints per cell type and demonstrates a progressive increase in MV-specific cell death with increasing transformation. MV-mediated cell killing was minimal in hTERT cells, where even at 72 hpi, fewer than 5% of the cells had died, compared to more than 60% cell death in 4+V and 5H at the same timepoint. Figure 2b shows fluorescence microscopy at the same timepoints after infection with MV-GFP; MV-induced syncytia were small and barely evident in hTERT but copious and large in transformed 3H, 4+V and 5H MSCs following MV infection.

Consistent with this, representative one step viral growth curves (figure 2c) showed that MV replication and release correlated with progressive transformation. In figure 2d, a comparison of the peak titres of cell-associated and supernatant MV (shown as mean and SEM of 3 independent replicates) shows a 2-3 log difference between hTERT/3H and 4+V/5H cells. We found no significant difference in MV receptor (SLAM, CD46 or Nectin-4) expression across the stages of transformation, ruling this out as potential mechanism for variable MV-permissiveness (supplementary figure S2). Taken together, clear difference in MV replication which were unrelated to density of receptor expression suggest that the model of stepwise transformation of

human BM-MSCs is good model for further elucidating mechanisms of MV-mediated oncolysis.

Differential production of type 1 IFN by MSCs in response to oncolytic MV

Production of type 1 IFN is essential for the induction of normal anti-viral immune responses, and results in the expression of a series of interferon-stimulated genes (ISGs). To determine whether differential interferon responses to oncolytic MV infection play a role in MV susceptibility, we quantified IFNα and β from tissue culture supernatants after infection. Only primary, unmodified normal human MSC control cells, produced any IFNα in response to MV infection (figure 3a). In comparison, IFNβ was produced by all MSCs following infection, but the level was inversely correlated to the transformational stage. Whilst primary MSCs (683 pg/ml) and hTERT cells (560 pg/ml) produced IFNβ at 24hpi, the more transformed MSCs only started to produce any IFNβ at 48hpi, with a maximum of 98 pg/ml, 34 pg/ml and 42 pg/ml in 3H, 4+V and 5H cells, respectively. This suggests that although all the MSCs were capable of mounting a type 1 IFN response, the magnitude and timing of the response is very different in the MV-resistant MSC compared to their malignant counterparts.

In order to determine whether the deficiency of IFNβ production could account for the increased susceptibility to MV infection and MV-mediated oncolysis, we asked whether it was possible to ‘rescue’ the highly MV-susceptible cells with exogenous interferon by adding IFNβ 16 hours prior to infection, followed by quantification of viral replication by qRT-PCR for the MV-N gene and assessment of cell viability at 30 hpi. As shown in figures 3b and 3c., IFNβ pretreatment reduced viral replication and

increased cell viability in 5H cells in a dose-dependent manner with the steepest increase at the lowest dose of IFNβ. The impact on viability in hTERT control cells was very modest.

In order to confirm downstream IFN pathway activation, we investigated the phosphorylation status of STAT1 and the expression of total STAT1 and IRF9 proteins by immunoblotting using cell lysates collected at 24hpi and compared to control, uninfected cells. STAT1 phosphorylation occurred in all MSCs in response to MV infection, more strongly in hTERT as shown in figure 3d (representative blot) and 3e (densitometry from *n*=3 blots). While endogenous STAT1 was expressed at higher basal levels in hTERT compared to the other cells, MV infection significantly increased STAT1 expression in 4+V and 5H cells. Similarly, IRF9 protein expression was induced in all MSCs following MV infection with a statistically significant increase observed for 3H cells (figures 3d and 3e). The time course of MV-stimulated STAT1 phosphorylation was determined in the most MV-susceptible 5H cells and compared with the most MV-resistant hTERT cells (figure 3f). STAT1 phosphorylation was not detected until 24hpi in 5H compared to a brisk response beginning at 4hpi in hTERT cells. The delayed STAT1 phosphorylation in 5H compared to hTERT cells parallels the pattern observed for IFNβ production.

RNA sequencing and qRT-PCR reveal differential baseline expression levels of genes involved in the type 1 IFN pathway response in MV-resistant and MV-susceptible MSCs

To gain a more global understanding of host responses and identify candidate genes, which could potentially be associated with increased susceptibility to oncolytic MV infection in this model, gene expression profiling by RNA-seq was performed using total RNA extracted from uninfected and MV-infected hTERT and 5H cells. We reasoned that the optimal timepoint was 24hpi, given that the MV-stimulated immune response was clearly underway by the time in both cell types, yet the MV-specific cell death was still minimal. Gene selection criteria were based on log_2fold change>1 and $p_{adjusted}$ <0.05. At baseline, a total of 4,902 differentially expressed genes (DEGs) were identified between hTERT and 5H cells with 2,438 upregulated genes and 2,464 downregulated genes relative to hTERT cells as shown the volcano plot in figure 4a. Reactome pathway enrichment analysis of genes significantly downregulated by more than 3-folds in 5H compared to hTERT cells revealed a number of enriched pathways, out of which type 1 IFN signaling was among the top ten, indicating significant baseline variability in immune-related functions (figure 4b). Upon MV infection, a total of 795 DEGs (155 downregulated and 640 upregulated) were identified in MV-infected hTERT compared to uninfected controls. In 5H cells, 1,109 DEGs were identified (75 downregulated and 1034 upregulated) in MV-infected compared to uninfected 5H cells as shown in the volcano plots in figure 4c. We selected the DEGs that were commonly upregulated in both cell lines following MV infection (394 genes) and analysed them for pathway enrichment. (figure 4d). The pathways most affected by MV infection were, not surprisingly, mostly related to the immune system and included antigen presentation and interferon signalling. Given our prior finding of the clear relevance of the type 1 IFN pathway in oncolytic MV susceptibility and noting that RNA-seq also identified it as one of the most differentially activated pathways, we validated RNA-seq data in

separate experiments, by quantifying the expression of 84 genes involved in the type 1 IFN signalling pathway in uninfected hTERT and 5H cells using the RT^2 Profiler PCR array, done as N=3 independent experiments. The results are presented as a heatmap in figure 5a and supplementary figure S3. In the absence of infection, 18 of the 84 genes analysed were significantly differentially expressed between hTERT and 5H at baseline (fold change >2, p value<0.05) The largest down-regulation was found in the gene encoding *IFITM1* (225.62-fold regulation, p= 0.045), followed by *MX2* (-38.09-fold regulation, p=0.002) and *MX1* (-15.76-fold regulation, p=0.049) (figure 5b and supplementary table S1). Figure 5c shows the changes in the 84 genes 24hpi; genes repressed in 5H cells relative to hTERT are induced to levels equivalent to, or greater than, those observed in hTERT cells at baseline, suggesting that the differential susceptibility to MV infection is due to baseline differences in type 1 IFN pathway gene expression, rather than the inability of 5H cells to deploy that pathway upon challenge. The *IFITM* genes seemed to show the greatest changes. The expression profiles of these genes before and after MV infection are plotted separately, in figure 5d. *IFTIM1* was greatly and very significantly downregulated in 5H compared to hTERT (-225.6-fold regulation) and was induced upon MV infection by 8.37-fold and 134.92-fold in hTERT and 5H cells, respectively (figure 5d).

IFITM1 expression is correlated with progressive MSC transformation

The viral-restricting properties of IFITM1 proteins have been documented for a number of viruses but not specifically for MV. Due to its prominence in our findings, we focused on *IFITM1* as a candidate gene for potentially restricting MV infection. We analysed our full set of sequentially transformed MSCs for basal expression of *IFITM1* in the absence of MV infection by qRT-PCR (figure 6a). *IFITM1* expression

was significantly lower in the more transformed MSCs compared to hTERT cells, with 4+V cells exhibiting the largest downregulation (-988.18-fold). *IFITM1* expression was significantly induced in all MSCs at 24h after MV infection to levels correlated with the MSCs transformational stage, with hTERT cells exhibiting the lowest induction (2.88-fold) and 5H showing the highest induction (771.4-fold) (figure 6b). IFITM1 protein expression was evaluated at immunoblotting using cell lysates collected at 24hpi. Interestingly, results did not follow the gene expression results; MV infection strongly induced IFITM1 protein expression in hTERT, and to lesser extent in 3H and 5H cells. IFITM1 expression was almost undetectable in 4+V cells (figure 6c).

We hypothesized that, if *IFITM1* was an important factor restricting MV oncolysis in non-transformed cells, overexpression in transformed 5H cells would restrict the ability oncolytic capacity of MV. Hence, we stably overexpressed *IFITM1* in the highly MV-permissive 5H cells (termed 5H-IFITM1) by retroviral vector transduction. Cells were FACS-sorted by red fluorescent protein (RFP) expression (figure 6d). Quantification of *IFITM1* gene expression by qRT-PCR in transduced 5H cells showed that more than a 10,000-fold overexpression was obtained compared to control non-transduced 5H cells. Compared to hTERT cells, 5H-IFITM1 showed a 9.2-fold upregulation in IFITM1 expression (figure 6e). Overexpression of IFITM1 in uninfected, non-MV infected 5H cells was confirmed by western blotting (figure 6f).

Restoration of *IFITM1* expression restricts oncolytic MV infection in transformed cells

In order to determine the extent to which restoration of *IFITM1* could restrict MV infection in transformed cells, 5H-IFITM1 and control 5H cells were infected with MV-NSe (MOI of 1.0) and assessed for cell viability, syncytia formation and viral replication. As shown in figure 7a, *IFITM1* overexpression increased cell viability after MV infection by 50% at 24hpi. By 48hpi, the majority of the 5H and 5H-IFITM1 cells had been succumbed to MV oncolysis. *MV-N* expression was significantly reduced in 5H-IFITM1 compared to 5H at 24 hours (figure 7b). MV-induced syncytia formation was only modestly affected by IFITM1 overexpression at 24 hours and not at all by 48 hours (figure 7c). We next measured the expression of IFITM1 following MV infection in non-transduced 5H cells, 5H-IFITM1 cells and hTERT control cells. Both hTERT and 5H showed an increase of IFITM1 expression at 24hpi, with hTERT cells exhibiting a smaller induction. However, the level of IFITM1 expression in 5H-IFITM1 cells remained unchanged following MV infection, suggesting that baseline IFITM1 expression is the most appropriate correlate of resistance to oncolytic MV infection in non-transformed cells (figure 7d). Interestingly, despite finding no difference in the relative expression of *IFITM1* mRNA after MV infection of 5H-IFITM1 cells, protein expression clearly increased as shown in figure 6f. There are presumably a number of reasons for this reported in the literature, including post-transcriptional modifications, degradation of the mRNA and the "translation on demand" where mRNA is preferentially translated under stressful conditions to ensure that the protein is rapidly available in response to signals.[20,21] Taken together, using a stromal cell model of sequential transformation, our data indicate that the lack of an adequate interferon response is a key reason for the oncolytic selectivity of the vaccine strain of MV. In particular, we have identified IFITM1 as a restriction factor for oncolytic MV.

Discussion

The mechanisms by which attenuated, vaccine strain MV exerts its oncolytic effects remain to be fully elucidated. In a well-characterized model of stepwise cellular transformation of BM-derived MSC, we can clearly show that productive infection leading to higher levels of MV-mediated cell killing occurred only in more highly transformed cells. We were able to use this model to probe the contribution of the type 1 IFN pathway at different stages of transformation. Whilst other groups have studied MV oncolysis in MV-permissive and non-permissive cancer cell lines or xenografts, our study allows for the direct comparison between transformed cells and their normal healthy counterparts. However, we have broadly similar findings. Berchtold *et al*., (2013) showed that in sarcoma cell lines, the upregulation of *RIG-I* and *IFIT1*, as well as STAT1 phosphorylation in response to MV infection were correlated with their resistant phenotype.[22] Furthermore, Achard *et al.*, (2015) showed that replication of oncolytic MV in malignant pleural mesothelioma cell lines was restricted in cells with intact IFN signalling.[23] Upon examining antiviral responses in MV-resistant and MV-permissive patient-derived glioblastoma xenografts (PDXs) using genome expression profiling, Kurokawa *et al.,* (2018) showed that constitutive activation of the IFN pathway was critical for MV replication.[18] Our data show that type 1 IFN production, was closely correlated with progressive transformation with cells at late stages of transformation producing lower levels of IFNβ in response to oncolytic MV infection compared to primary and hTERT MSCs. The observation that pre-treating MV-susceptible 5H cells with exogenous IFNβ restored resistance to MV-mediated oncolysis suggested that this was indeed a

biologically plausible mechanism. Consistently, we observed a muted but also very delayed type 1 IFN response with increasing transformation, which was mirrored by the timecourse of STAT1 phosphorylation, which was already maximal at 4 hours, post infection in hTERT cells but only began at 24 hours in the fully transformed 5H cells.

Transcriptomic evaluation allowed us to gain a more global view of the impact of oncolytic MV in transformed and non-transformed cells. 5H cells expressed significantly lower basal levels of genes involved in the interferon gamma pathway, the interferon alpha/beta pathway and the antigen presentation and processing pathways than hTERT cells. However, oncolytic MV infection triggered the upregulation of genes involved in immune responses including antigen presentation and interferon signalling in both cell types. In both the RNA-sequencing and the RT^2 profiler validation experiments, genes that were basally repressed in 5H cells, relative to hTERT, were induced by MV infection to levels equivalent to, or greater that those that had been observed in hTERT cells at baseline. However, despite the induction of an immune response in 5H cells, the viral replication outpaced the antiviral response, suggesting that the differential susceptibility to MV infection is due to significant baseline differences in type 1 IFN pathway gene expression leading to a delayed response, rather than the inability of 5H cells to deploy those pathways upon challenge.

Unsurprisingly, given the importance of the interferon pathway, a number of ISGs such as *OAS2*, *PKR* and *MX1/2* have been reported as viral restriction factors.[24] However, the majority of ISGs remain to be functionally characterized and it is of

interest to know if they might serve as predictive biomarkers for identifying patients who are more likely to response to oncolytic MV virotherapy. Recently, Kurokawa *et al*. (2019), identified the ISG, *RSAD2*, as an inhibitor of oncolytic MV replication by blocking viral release in both 293T cells and SR-B2, an ovarian cancer cell line.[25] Our RNA-seq results showed that *RSAD2* was also downregulated in 5H compared to hTERT cells, however this was not statistically significant, suggesting that different ISGs may function in a cell type-specific manner. By contrast, our data highlighted interferon-inducible transmembrane protein 1 (*IFITM1*) as the foremost downregulated ISG in 5H transformed cells compared to non-transformed hTERT cells at baseline. Following oncolytic MV infection *IFITM1* expression increased only modestly in hTERT cells compared to a much higher, significant 771-fold increase in 5H cells, suggesting it may play a role in the selectivity of MV-mediated oncolysis in transformed cells. Interestingly, even though MV infection resulted in increased *IFITM1* transcription in transformed MSCs, IFITM1 protein expression was not detected in the same cells, strongly implying the existence of post-transcriptional modifications. This observation is possibly a compensatory mechanism that contributes to the MV-susceptible phenotype of these cells. In support of this notion, mircoRNA-mediated regulations were reported to inhibit IFITM1 protein expression following infection with Kaposi's sarcoma-associated herpesvirus[26] and hepatitis C virus.[27]

The antiviral activities of IFITM family members, *IFITM1*, *IFITM2* and *IFITM3* were demonstrated by a number of studies. *IFITM1* particularly restricted enveloped RNA viruses, including hepatitis C virus,[28-30] HIV,[31] influenza virus A H1N1,[32] Zika virus,[33] respiratory syncytial virus (RSV),[34, 35] mumps virus, Newcastle disease virus (NDV),

human metapneumovirus and parainfluenza virus.[34] The viral restriction properties of *IFITM1* on a number of viruses that enter cells via the plasma membrane were recently investigated by Smith *et al*. (2019). A small but significant effect of *IFITM1* overexpression was observed on the replication of strains of MV that are currently not used as cancer therapies, namely the Edmonston-Zagreb strain[36] and a recombinant MV strain with a replaced P gene[37] which has been shown to be competent for immune evasion.[38] A proposed mechanism of action for the IFITM proteins in this regard is that the fluidity of cellular membranes can be altered, preventing fusion with the infecting virus envelope. Consistent with this, our own data do show fewer and smaller syncytia in hTERT versus 5H cells whereas virus release does not appear to be impacted, as we observed viral titres in the supernatants which were consistent with titres in the lysates at all of the transformational stages.

Consistent with a block to entry, our studies showed a 50% increase in cell viability after 24 hours of infection in *IFITM1*-overexpressing 5H cells relative to control 5H cells. Moreover, *IFITM1* overexpression altered the ability to establish an infection, as monitored by the significant decrease in expression of MV-N viral transcripts. However, by 48 hours post infection, multinucleated syncytia were readily apparent and cell killing reached levels similar to those in control 5H cells, suggesting that the antiviral effects of *IFITM1* were indeed limited to early stages of infection.

Taken together, we have used a model of sequential transformation to show that a reduction in function of the type 1 IFN pathway is a major contributor to the selectivity of MV-mediated oncolysis for transformed cells. Our data have also

identified *IFITM1* as an oncolytic MV restriction factor. The mechanisms of action of IFITM1 remain to be determined. Co-factors which may be acting in a combined manner with IFITM1 may also be identified from our data and that of others. Mechanistic insights into MV oncolysis will assist with candidate tumor selection, trial design and also help direct potential therapeutic combinations.

Methods

Cell culture:

Vero (African green monkey kidney cells, ATCC) were cultured in Dulbecco's modified eagle medium (DMEM; Invitrogen) supplemented with 5% fetal bovine serum (FBS; Gibco), L-glutamine (2mM; Gibco) and 100units/ml penicillin-streptomycin (Gibco). Primary mesenchymal stromal cells (MSCs) were obtained from healthy bone marrow (BM) samples after written consent. BM samples were filtered through a 40μM cell strainer (Becton Dickinson LTD) and BM mononuclear cells were isolated by density gradient centrifugation using Ficoll-Paque (Amersham Biosciences). All MSCs were cultured in MesenCult MSC basal medium with MesenCult stimulatory supplements (StemCell technologies), 5% FBS, L-glutamine, penicillin-streptomycin and 1ng/ml recombinant basic human FGF (R&D systems). Phoenix AMPHO cells (ATCC) were grown in DMEM supplemented with 10% FBS, penicillin-streptomycin and L-glutamine. All cells were maintained in a 37℃ humidified 5% CO2 incubator.

Model of sequentially transformed BM-MSCs:

The transformed human bone marrow-derived mesenchymal stromal cells (BM-MSCs) were developed and characterized elsewhere by Funes *et al* [19]. Briefly, human BM-MSCs were sequentially infected with retroviral particles carrying the following expression vectors: pBABE-puro-EST2 (hTERT expression), pLXSN-neo-E6E7 (inactivation of p53 and Rb) to generate 3H cells, pBABE-zeo-ST (introduction of SV40 small T antigen) to generate 4+V cells and pWZL-hygro-RasV12 (expression of oncogenic H-Ras^{V12}) to generate 5H cells. Following serial retroviral infections, drug selection with puromycin (100µg/ml), neomycin (300µg/ml), Zeocin (50µg/ml) and hygromycin (100µg/ml), respectively, was used to purify cell populations. The validity of this model was demonstrated by anchorage-independent growth, tumour growth in immunodeficient mice and gene expression profiles consistent with transformed cells.[19]

Cell counting and viability assays:

Cell viability was measured using trypan blue (Sigma Aldrich, Poole, UK) dye exclusion. Viability after MV infection was expressed as a percentage of non-infected cell viability.

Propagation and titration of MV:

Live-attenuated vaccine strain of measles virus (MV-NSe) and MV expressing recombinant green fluorescent protein (MVNSe-GFP) were propagated on Vero cells. Vero cells were plated in 14-cm plates and infected at a multiplicity of infection (MOI) of 0.01 in Opti-MEM (Gibco). When 80%-90% cytopathic effect was observed, the virus was harvested by scraping the cells and subjected to two freeze-thaw cycles to release cell-associated viral particles. This was followed by high-speed

centrifugation (4000 rpm for 5 min at 4℃) to remov e cell debris. Aliquots were stored at -80℃.Viral titers were determined by the end-po int infectivity assay. The 50% tissue culture infected dose ($TCID_{50}$) of MV stock was calculated using the modified Kärber formula.[39]

MV infections:

For MV infection of adherent Veros and MSCs, cells were washed once with PBS and then inoculated with virus in Opti-MEM (Gibco) at a multiplicity of infection (MOI) of 1.0 in all experiments. Mock-infected cells were washed once and inoculated with Opti-MEM only. Cells were incubated for two hours at 37℃ before removal of the inoculum and replacement with fresh media. In conditions where cells were cultured in the presence of exogenous IFNβ, cells were pre-treated with concentrations ranging from 50-1000 U/ml recombinant IFNβ (Millipore, UK, IF014) for 16 hours before infection with MV-NSe at an MOI of 1.0.

MV receptor expression by flow cytometry:

A total of 1-10x10^5 cells per aliquot were incubated with a FITC-labeled anti-human CD46 antibody (R&D systems), or phycoerythrin (PE)-labeled anti-human CD105 antibody (BD Biosciences), or PE-labeled anti-human nectin-4 (R&D systems) at 4℃ in the dark for 30 minutes. Cells were then washed and resuspended in PBS. Samples were acquired on a BD FACSAria or LSR II flow cytometer (Becton Dickinson, Oxford, UK) with 5000-10,000 events being recorded and analysed with FlowJo (Tree Star). Results are expressed as mean fluorescence intensity (MFI). As a positive control for CD46 surface expression, Raji cells were used. Isotype-stained cells were used as negative controls.

Enzyme-linked immunosorbent assay:

MSCs were plated at a density of $5x10^5$ per well in 6-well plates and infected with MV-NSe. At 24 and 48hpi, tissue culture supernatants were collected and stored at -80℃. Quantification of IFN α and IFNβ was performed using VerikineTM Human IFN alpha Multi-Subtype ELISA (PBL Assay Science, NJ) and VerkineTM Human IFN beta (PBL Assay Science, NJ) kits, respectively, according to the manufacturer's protocol.

Quantitative real time PCR:

MSCs were infected in 6-well plates at $3x10^5$ cells per well. Total cell RNA was extracted using the TRIzol (Invitrogen) method 24 and 48 hours post infection. Quantification of RNA samples concentration and purity was achieved by measuring UV-light absorbance at 260nm (A260) and 280nm (A280) using the NanodropTM 1000 spectrophotometer (Thermo Fisher Scientific). For each sample, 0.4-1μg total RNA was reverse transcribed using SuperScriptTM III reverse transcriptase (Invitrogen) according to the manufacturer's protocol and 60ng of the synthesized cDNA product was used in triplicate reactions of quantitative PCR (qPCR). qPCR reactions were performed by mixing cDNA with 12.5μl of 2X TaqMan universal PCR master mix (Applied Biosystems) and 1.25μl of 20X TaqMan gene-specific primer and a probe mix (TaqMan gene expression assay, Cat number 4331182 and 4331348; Applied Biosystems) to a final reaction volume of 25μl. The TaqMan assays used as follows: IFITM1 (Hs00705137_s1), GAPDH (Hs02786624_g1) and custom MV-N assay (ID AIY896X) (all from Applied Biosystems). PCR reactions were carried out on an ABI 7500 fast real-time PCR system (Applied Biosystems)

according to the following conditions: 95℃ for 10 minutes, 40 cycles of 95℃ for 15 seconds and 60℃ for 1 minute. GAPDH was used as a housekeeping gene for all assays. Samples were run in triplicate for each gene and non-template controls (NTC) were included for each primer set. PCR cycle number at threshold is represented as Ct. Relative expression level of genes of interest was calculated using the comparative 2−ΔΔCt formula and expressed in fold change as compared to corresponding uninfected control cells.

RT^2 Profiler PCR array:

Total RNA was analysed using the Human Type 1 Interferon Response RT^2 Profiler PCR Array (Cat number PAHS-016Z; Qiagen), which profiles the expression of 84 gene transcripts that are known to be involved in the type 1 IFN response, as well as the expression of five housekeeping genes (*ACTB, B2M, GAPDH, HPRT1 and RPLP0*). In addition, one well contains a genomic DNA control, three wells contain reverse-transcription controls and three wells contain positive PCR control. For each sample, 0.5µg RNA was reverse transcribed into cDNA using the RT^2 First Strand Kit (Qiagen, UK). The cDNA was then mixed with the RT^2 SYBR Green Mastermix (Qiagen, UK) and nuclease-free water. Next, 25ul of the PCR mix was added to each well of the 96-well plate. All steps were done according to the manufacturer's instructions. The qPCR reaction was run on an ABI 7500 (fast block) according to the following conditions: 95℃ for 10 minutes, followed by 40 cycles of 95℃ for 15 seconds and 60℃ for 1 minute. Data analysis was conducted using a software-based tool (Qiagen's GeneGlobe Data Analysis Center). The exported Ct values for each well were uploaded into the software, which performed fold-change calculations

based on 2−ΔΔCt method. Expression levels were quantified relative to the values obtained for housekeeping genes.

Immunoblotting:

MSCs were infected in 6-well plates at a density of 3 x10^5 cells per well. At specific timepoints post infection, cells were washed once with cold PBS before adding 100µl RIPA cell lysis buffer (Sigma-Aldrich) with complete mini protease inhibitor cocktail tablets (Sigma-Aldrich, Roche) and harvested. After incubation on ice for 30 minutes, cell lysates were centrifuged at 14,000 rpm for 5 minutes at 4℃ to pellet the cell debris. The supernatant was aliquoted and stored at -80℃ until use. Protein concentrations were determined using the BCA (Bicinchoninic Acid) protein assay kit (Sigma-Aldrich). Equal amounts of protein (30µg-50µg) were mixed with loading dye, incubated at 70℃ for 10 minutes to denature the proteins and then loaded onto 4-12% Bolt Bis-Tris Plus gels (Thermo Fisher Scientific). Gels were subject to electrophoresis at 200V for 22 minutes. After SDS-PAGE, the proteins were transferred to nitrocellulose membranes using the iBlot$_{TM}$ 2 Gel Transfer Device (Thermo Fisher Scientific). Membranes were blocked in 3% non-fat dry milk in Tris-buffered saline (TBS) with Tween-20 (TBS-T) for one hour at room temperature. This was followed by incubation with the following primary antibodies: rabbit anti-STAT1 (Cell signaling Technology CST, #9172), rabbit anti-phospho-STAT1 (Tyr701, CST, #7649), rabbit anti-IRF9 (CST, #28492), mouse anti-GAPDH (CST, #97166), rabbit anti-IFITM1 (Proteintech, 11727-3-AP and CST, #13126), and mouse beta-tubulin (Thermo Fisher, BT7R). Primary antibodies were diluted 1:1,000 in 3% BSA or 3% milk in TBS-T at 4℃ overnight. Membranes were washed three times for five minutes with TBS-T followed by incubating with anti-mouse IgG or anti-rabbit

horseradish peroxidase-conjugated IgG secondary antibodies (Promega) for one hour at room temperature. All secondary antibodies were diluted 1:50,000 in 3% milk in TBS-T. Membranes were washed again at this point with TBS-T to remove any unbound antibodies. Immunodetection was performed with Amersham ECL prime western blotting detection reagent (GE Healthcare Life Sciences) using the ImageQuant^{TM} Las 4000 system (GE Healthcare Life Sciences). Densitometry of bands was carried out using ImageJ and was normalized to the expression level of the relevant loading control.

RNA sequencing and differential expression analysis

TRIzol reagent (Invitrogen) was used to extract total RNA from uninfected or MV-infected hTERT and 5H MSCs at 24hpi. Samples were processed using the KAPA mRNA library prep hyper kit and sequenced on the Illumina NextSeq 500 (Illumina) by the UCL Genomics facility (London, UK). RNA-seq data was analysed for differential gene expression using the DESeq2[40,41] and SARTools (developed at PF2- Institut Pasteur) R packages. DESeq2 provides statistical methods for determining differential expression data using a model based on the negative binomial distribution. Volcano plots were generated by R (R Core Team, 2014) to display differential gene expression results between two comparison groups. Each point represents the average value of one transcript in three replicate experiments. Differentially expressed genes (DEGs) were selected based on an absolute log2 fold change >1 and an adjusted p value<0.05. Red and green dots represent upregulated and downregulated genes compared to control, respectively. Grey dots represent non-significantly regulated genes. Pathway enrichment analysis was performed on

DEGs using Reactome (www.reactome.org [42]). RNA-seq data have been deposited in the GEO repository under the accession number GSE131840.

Construction of the IFITM1–expressing vector:

The full-length *IFITM1* cDNA was PCR-amplified from the pCMV-HA-IFITM1 plasmid (a gift from H. Hang and J. Yount, Addgene plasmid #58399), using primers tailed with BamHI and XhoI linker restriction sites at the 5' and 3' ends, respectively (Sigma Aldrich).

Forward primer: 5'-tctgatGGATCCtctgatATGCACAAGGAGGAACAT-3'

Reverse primer: 5'- GAAAAACGGGGTTACTAGtctgatCTCGAGtctgat-3'

The amplified PCR fragment (378 basepairs) was cloned into a pCR II-TOPO vector using the TOPO TA cloning kit (Invitrogen) according to the manufacturer's protocol and sequenced for confirmation (Eurofins) before being cloned into the retroviral vector MSCV-IRES-mRFP (a gift from Charles G. Mullighan, St. Jude Children's Research Hospital, Memphis, USA; figure S1). To obtain the overexpressing construct, pCR II-TOPO-IFITM1 and MSCV-IK6-IRES-mRFP plasmids were both digested using BamHI high fidelity and XhoI restriction enzymes (New England BioLabs, NEB). The digested vectors were separated by electrophoresis using 2% agarose gels and the target IFITM1 insert and MSCV backbone were purified using the QIAex II gel purification kit (Qiagen). The purified fragments were ligated using T4 DNA ligase (NEB) and transformed into One Shot DH5α-T1^{R} *E.coli* competent cells (Invitrogen). The recombinant plasmid was isolated from bacterial pellets using the HiSpeed Plasmid Midi kit (Qiagen). Agarose gel electrophoresis confirmed the presence of the correct IFITM1 insert and the sequence was verified (Eurofins

Genomics, UK). A schematic representation of the construction of MSCV-IRES-RFP-IFITM1 plasmid is illustrated in supplementary figure S1.

Retroviral transduction of 5H MSCs

For the preparation of retroviral vector particles, Phoenix AMPHO cells were co-transfected with the appropriate plasmids using a Fugene® high-density transfection reagent (Roche) method. Briefly, $2x10^6$ Phoenix AMPHO cells were plated into 10cm petri dishes in 8ml fresh media and incubated at overnight. On the following day, the transfection mix was prepared by first adding 10µl Fugene and 150µl OptiMEM, this is solution A. Solution B was prepared by adding 1.5µg pCL-ampho retrovirus packaging vector (Imgenex), 2.6µg MSVC-IFITM1-IRES-mRFP plasmid and adjusting the volume to 50ul with dH2O. The DNA mix was then added to the Fugene® solution, mixed by gentle pipetting, and incubated at room temperature for 15-20 minutes. The liposomal complexes were added directly to the Phoenix AMPHO cells and then returned to the incubator. Three days after transfection, medium was replaced with 5ml of fresh DMEM media. Retroviral supernatants from the transfected packaging cells were ready to be used for transduction on the following. Collected supernatants were spun at 1500rpm for 5 minutes to remove remaining cells and cell debris and used for infection of 5H MSCs. FACS analysis was performed for sorting RFP-positive cells.

Statistical analysis:

Statistical analysis and graph plotting were performed using GraphPad Prism 5.0 (Graphpad Software Inc.). Graph data are represented as mean ± SEM. For comparisons involving two groups, paired or unpaired Student's t-tests (two-tailed)

were used for statistical analysis. P values less than 0.05 were considered to be statistically significant. * $p<0.05$, ** $p<0.01$, *** $p<0.001$. The number of independent experiments performed is indicated by *n* in the figure legends.

Acknowledgements

We thank all the members of the Fielding lab for their feedback on this project. We thank David Gullinghan (St Jude's Children's hospital) for providing the MSCV-IK6 plasmid. We thank Juan M Funes and Chris Boshoff for the transformed MSC model. We thank UCL Genomics for the RNA sequencing. This work was funded by a grant to S.A. from the King Abdullah International Research Center, Riyadh, Saudi Arabia.

Author contributions

S.A. and A.Z.C. designed experiments, performed experiments and interpreted data. A.K.F. and S.A. wrote the paper. D.L. and S.A. performed RNA-seq analysis. A.D., R.B., D.O., K.B. and R.M. provided technical assistance and contributed to the interpretation of the results. A.K.F. conceived the project, critically evaluated experiments and supervised the study. The authors declare no conflicts of interest.

References

1. Prestwich, R.J., Harrington, K.J., Pandha, H.S., Vile, R.G., Melcher, A.A., and Errington, F. (2008). Oncolytic viruses: a novel form of immunotherapy. Expert Rev Anticancer Ther 8: 1581-1588.
2. Msaouel, P., Opyrchal, M., Dispenzieri, A., Peng, K.W., Federspiel, M.J., Russell, S.J., et al. (2018). Clinical Trials with Oncolytic Measles Virus: Current Status and Future Prospects. Curr Cancer Drug Targets 18: 177-187.
3. Moss, W.J., and Griffin, D.E. (2006). Global measles elimination. Nat Rev Microbiol 4: 900-908.

4. Naniche, D., Varior-Krishnan, G., Cervoni, F., Wild, T.F., Rossi, B., Rabourdin-Combe, C., et al. (1993). Human membrane cofactor protein (CD46) acts as a cellular receptor for measles virus. J Virol 67: 6025-6032.
5. Dorig, R.E., Marcil, A., Chopra, A., and Richardson, C.D. (1993). The human CD46 molecule is a receptor for measles virus (Edmonston strain). Cell 75: 295-305.
6. Tatsuo, H., Ono, N., Tanaka, K., and Yanagi, Y. (2000). SLAM (CDw150) is a cellular receptor for measles virus. Nature 406: 893-897.
7. Noyce, R.S., Bondre, D.G., Ha, M.N., Lin, L.T., Sisson, G., Tsao, M.S., et al. (2011). Tumor cell marker PVRL4 (nectin 4) is an epithelial cell receptor for measles virus. PLoS Pathog 7: e1002240.
8. Muhlebach, M.D., Mateo, M., Sinn, P.L., Prufer, S., Uhlig, K.M., Leonard, V.H., et al. (2011). Adherens junction protein nectin-4 is the epithelial receptor for measles virus. Nature 480: 530-533.
9. Navaratnarajah, C.K., Oezguen, N., Rupp, L., Kay, L., Leonard, V.H., Braun, W., et al. (2011). The heads of the measles virus attachment protein move to transmit the fusion-triggering signal. Nat Struct Mol Biol 18: 128-134.
10. Anderson, B.D., Nakamura, T., Russell, S.J., and Peng, K.W. (2004). High CD46 receptor density determines preferential killing of tumor cells by oncolytic measles virus. Cancer Res 64: 4919-4926.
11. Miest, T.S., Frenzke, M., and Cattaneo, R. (2013). Measles virus entry through the signaling lymphocyte activation molecule governs efficacy of mantle cell lymphoma radiovirotherapy. Mol Ther 21: 2019-2031.
12. Stojdl, D.F., Lichty, B., Knowles, S., Marius, R., Atkins, H., Sonenberg, N., et al. (2000). Exploiting tumor-specific defects in the interferon pathway with a previously unknown oncolytic virus. Nat Med 6: 821-825.
13. Plumet, S., Herschke, F., Bourhis, J.M., Valentin, H., Longhi, S., and Gerlier, D. (2007). Cytosolic 5'-triphosphate ended viral leader transcript of measles virus as activator of the RIG I-mediated interferon response. PLoS One 2: e279.
14. Ikegame, S., Takeda, M., Ohno, S., Nakatsu, Y., Nakanishi, Y., and Yanagi, Y. (2010). Both RIG-I and MDA5 RNA helicases contribute to the induction of alpha/beta interferon in measles virus-infected human cells. J Virol 84: 372-379.
15. Berghall, H., Siren, J., Sarkar, D., Julkunen, I., Fisher, P.B., Vainionpaa, R., et al. (2006). The interferon-inducible RNA helicase, mda-5, is involved in measles virus-induced expression of antiviral cytokines. Microbes Infect 8: 2138-2144.
16. Schoggins, J.W., and Rice, C.M. (2011). Interferon-stimulated genes and their antiviral effector functions. Curr Opin Virol 1: 519-525.
17. Schneider, W.M., Chevillotte, M.D., and Rice, C.M. (2014). Interferon-stimulated genes: a complex web of host defenses. Annu Rev Immunol 32: 513-545.
18. Kurokawa, C., Iankov, I.D., Anderson, S.K., Aderca, I., Leontovich, A.A., Maurer, MJ, et al. (2018). Constitutive Interferon Pathway Activation in Tumors as an Efficacy Determinant Following Oncolytic Virotherapy. J Natl Cancer Inst 110: 1123-1132.
19. Funes, J.M., Quintero, M., Henderson, S., Martinez, D., Qureshi, U., Westwood, C., et al. (2007). Transformation of human mesenchymal stem cells increases their dependency on oxidative phosphorylation for energy production. Proc Natl Acad Sci U S A 104: 6223-6228.

20. Greenbaum, D., Colangelo, C., Williams, K., and Gerstein, M. (2003). Comparing protein abundance and mRNA expression levels on a genomic scale. Genome Biol 4: 117.
21. Liu, Y., Beyer, A., and Aebersold, R. (2016). On the Dependency of Cellular Protein Levels on mRNA Abundance. Cell 165: 535-550.
22. Berchtold, S., Lampe, J., Weiland, T., Smirnow, I., Schleicher, S., Handgretinger, R., et al. (2013). Innate immune defense defines susceptibility of sarcoma cells to measles vaccine virus-based oncolysis. J Virol 87: 3484-3501.
23. Achard, C., Boisgerault, N., Delaunay, T., Roulois, D., Nedellec, S., Royer, P.J., et al. (2015). Sensitivity of human pleural mesothelioma to oncolytic measles virus depends on defects of the type I interferon response. Oncotarget 6: 44892-44904.
24. Sadler, A.J., and Williams, B.R. (2008). Interferon-inducible antiviral effectors. Nat Rev Immunol 8: 559-568.
25. Kurokawa, C., Iankov, I.D., and Galanis, E. (2019). A key anti-viral protein, RSAD2/VIPERIN, restricts the release of measles virus from infected cells. Virus Res 263: 145-150.
26. Hussein, H.A.M., and Akula, S.M. (2017). miRNA-36 inhibits KSHV, EBV, HSV-2 infection of cells via stifling expression of interferon induced transmembrane protein 1 (IFITM1). Sci Rep 7: 17972.
27. Bhanja Chowdhury, J., Shrivastava, S., Steele, R., Di Bisceglie, A.M., Ray, R., and Ray, R.B. (2012). Hepatitis C virus infection modulates expression of interferon stimulatory gene IFITM1 by upregulating miR-130A. J Virol 86: 10221-10225.
28. Wilkins, C., Woodward, J., Lau, D.T., Barnes, A., Joyce, M., McFarlane, N., et al. (2013). IFITM1 is a tight junction protein that inhibits hepatitis C virus entry. Hepatology 57: 461-469.
29. Raychoudhuri, A., Shrivastava, S., Steele, R., Kim, H., Ray, R., and Ray, R.B. (2011). ISG56 and IFITM1 proteins inhibit hepatitis C virus replication. J Virol 85: 12881-12889.
30. Narayana, S.K., Helbig, K.J., McCartney, E.M., Eyre, N.S., Bull, R.A., Eltahla, A., et al. (2015). The Interferon-induced Transmembrane Proteins, IFITM1, IFITM2, and IFITM3 Inhibit Hepatitis C Virus Entry. J Biol Chem 290: 25946-25959.
31. Lu, J., Pan, Q., Rong, L., He, W., Liu, S.L., and Liang, C. (2011). The IFITM proteins inhibit HIV-1 infection. J Virol 85: 2126-2137.
32. Brass, A.L., Huang, I.C., Benita, Y., John, S.P., Krishnan, M.N., Feeley, E.M., et al. (2009). The IFITM proteins mediate cellular resistance to influenza A H1N1 virus, West Nile virus, and dengue virus. Cell 139: 1243-1254.
33. Savidis, G., Perreira, J.M., Portmann, J.M., Meraner, P., Guo, Z., Green, S., et al. (2016). The IFITMs Inhibit Zika Virus Replication. Cell Rep 15: 2323-2330.
34. Smith, S.E., Busse, D.C., Binter, S., Weston, S., Diaz Soria, C., Laksono, B.M., et al. (2019). Interferon-Induced Transmembrane Protein 1 Restricts Replication of Viruses That Enter Cells via the Plasma Membrane. J Virol 93.
35. Zhang, W., Zhang, L., Zan, Y., Du, N., Yang, Y., and Tien, P. (2015). Human respiratory syncytial virus infection is inhibited by IFN-induced transmembrane proteins. J Gen Virol 96: 170-182.
36. Rennick, L.J., de Vries, R.D., Carsillo, T.J., Lemon, K., van Amerongen, G., Ludlow, M., et al. (2015). Live-attenuated measles virus vaccine targets dendritic cells and macrophages in muscle of nonhuman primates. J Virol 89: 2192-2200.

37. de Vries, R.D., Lemon, K., Ludlow, M., McQuaid, S., Yuksel, S., van Amerongen, G., et al. (2010). In vivo tropism of attenuated and pathogenic measles virus expressing green fluorescent protein in macaques. J Virol 84: 4714-4724.
38. Devaux, P., von Messling, V., Songsungthong, W., Springfeld, C., and Cattaneo, R. (2007). Tyrosine 110 in the measles virus phosphoprotein is required to block STAT1 phosphorylation. Virology 360: 72-83.
39. Kärber, G. (1931). Beitrag zur kollektiven Behandlung pharmakologischer Reihenversuche. Naunyn-Schmiedebergs Archiv für experimentelle Pathologie und Pharmakologie 162: 480-483.
40. Love, M.I., Huber, W., and Anders, S. (2014). Moderated estimation of fold change and dispersion for RNA-seq data with DESeq2. Genome Biology 15: 550.
41. Anders, S., and Huber, W. (2010). Differential expression analysis for sequence count data. Genome Biology 11: R106.
42. Fabregat, A., Sidiropoulos, K., Viteri, G., Forner, O., Marin-Garcia, P., Arnau, V., et al. (2017). Reactome pathway analysis: a high-performance in-memory approach. BMC Bioinformatics 18: 142.

Figure legends

Figure 1 Model of stepwise transformation of human bone marrow-derived mesenchymal stromal cells. Schematic diagram of MSC stepwise transformation (adapted from Funes *et al.* 2007), MSCs were named according to the number of oncogenes inserted by retroviral transduction. hTERT encodes the catalytic subunit of human telomerase and confers the cells extended lifespan *in vitro.* Human papilloma virus (HPV-16) E6 and E7 genes abrogate the functions of *p53* and *pRb* tumour suppressors, respectively. SV40 small T antigen leads to the stabilization of *c-Myc* by inactivating protein phosphatase 2A. Finally, the insertion of an oncogenic allele of *Ras (H-Ras*^{V12}) provides the acquisition of a constitutive mitogenic signal.

Figure 2 Susceptibility to MV-mediated oncolysis is positively correlated with progressive transformation of MSCs. (A) MSCs were infected with MV-NSe (MOI of 1.0) and cell viability was assessed by trypan blue exclusion at 24, 48 and 72 hours post infection (hpi). Data is expressed as a percentage of cell killing by MV relative to uninfected control cells (*n*=3). **(B)** Representative GFP and bright-field (BF) microscopy images of MSCs 24hpi, 48 hpi and 72hpi with MV-NSe-GFP (MOI of 1.0). Scale bar, 200μm **(C)** Tissue culture supernatants (red lines) and cell lysates (black lines) were harvested at the indicated time points post infection. Viral titrations were performed on Vero cells and are calculated as $TCID_{50}$ (pfu/ml) (*n*=3). Data is expressed as mean ± SEM. All results shown are representative of three independent experiments. (unpaired *t*-test, *p<0.05, **p<0.01, ***p<0.001). MV= measles virus, NS= not significant

Figure 3 Differential production of type 1 IFN by MSCs in response to oncolytic MV. (A) IFNα and IFNβ production levels as assessed by ELISA using tissue culture supernatants collected from all MSCs, including primary patient-derived MSCS, at 24hpi and 48hpi. Data is expressed as mean ± S.E.M of two independent experiments (*n*=2) with samples measured in duplicates. **(B)** *MV-N* mRNA expression levels as assessed by qRT-PCR for 5H cells pre-treated with different concentrations of exogenous IFNb for 16 hours prior to MV infection. Data shown are relative to housekeeping gene *GAPDH* and normalized to uninfected control cells. Data is expressed as mean ± S.E.M (*n*=3). **(C)** Cell viability of 5H cells following pre-treatment with IFNβ and MV infection was assessed by trypan blue exclusion at 30hpi. hTERT cells were used as a control. Results are reported as a percentage of cell viability relative to uninfected control cells. Data is expressed as mean ± S.E.M (*n*=3). **(D)** Immunoblotting of total STAT1, phosphorylated STAT1 (pSTAT1) and IRF9 using cell lysate of uninfected and MV-infected MSCs collected at 24hpi. Beta-tubulin or GAPDH were used as loading controls (*n*=3). **(E)** Densitometry analysis of blot in (D) performed by ImageJ. **(F)** Immunoblot analysis of pSTAT1 during the time course of MV infection in 5H cells and hTERT cells using cell lysates collected at the indicated timepoints. Cells stimulated with IFNβ (1000U/ml) for one hour were used as a positive control. Beta-tubulin and GAPDH expression were used as loading controls as indicated.

Figure 4 RNA sequencing reveals differential baseline gene expression in MV-resistant and MV-susceptible MSCs. RNA-seq was performed on total RNA was extracted from uninfected and MV-infected hTERT and 5H cells at 24hpi (A) Volcano plot of differentially expressed genes (DEGs) in 5H cells compared to

hTERT cells at baseline levels (*n*=3). Cut-off criteria for DEGs are absolute log_2 fold change>1 and $p_{adjusted}$ value <0.05. The y-axis displays the log_{10} p-value for each gene, while the x-axis displays the log_2 fold change for that gene relative to hTERT. Red dots indicate up-regulated genes, green dots indicate down-regulated genes and grey dots indicate non-significant relative to hTERT. **(B)** Genes down-regulated (more than 3-fold down-regulation, p-value <0.05) in 5H compared to hTERT cells were selected and analysed using the functional annotation tool in REACTOME. The top 12 enriched pathways (p value<0.001) are shown. **(C)** Volcano plots depicting DEGs after infection of (i) hTERT cells and (ii) 5H cells (compared to mock-infected control cells). **(D)** Venn diagram illustrating the overlap of genes found to be up-regulated in response to MV infection in both hTERT and 5H cells (absolute log_2 FC>1, $p_{adjusted}$ value<0.05) **(E)** REACTOME pathway enrichment analysis of the 394 up-regulated genes. The top ten pathways are represented in the bar plot (p value<0.001).

Figure 5 Genes involved in the type 1 IFN signalling pathway are repressed in 5H compared to hTERT cells and induced by MV infection. Gene expression of 84 genes was validated by a custom type 1 IFN RT^2 Profiler PCR array (*n*=3). **(A)** Heat map representation of array genes in uninfected hTERT and 5H cells. Green represents low expression level, and red represents high expression levels**. (B)** Gene expression profile showing differentially expressed genes in 5H compared to hTERT (absolute log_2FC>1 and p<0.05). Gene names are shown on the x-axis. Data is expressed as mean ± SEM. **(C)** Fold change in gene expression of the 84 analysed genes at basal levels and upon induction by MV infection. **(D)** Differential

expression of IFITM genes (*IFITM1*, *IFITM2* and *IFITM3)* before and after MV infection of hTERT and 5H cells. For *IFITM1*, hTERT vs. 5H *p=0.0338.

Figure 6 IFITM1 expression is correlated with progressive MSC transformation. **(A)** *IFITM1* mRNA expression in all MSCs as assessed by qRT-PCR. Data shown are relative to housekeeping gene *GAPDH* and normalized to hTERT cells (n=3). **(B)** *IFITM1* mRNA expression measured by qRT-PCR at 24hpi of all MSCs. Data shown are relative to housekeeping gene *GAPDH* and normalized to uninfected control cells (n=3). **(C**) Immunoblot showing IFITM1 protein expression at 24hpi in uninfected and MV-infected MSCs. Beta-tubulin is used as a loading control. **(D)** Histograms of FACS analysis of the expression levels of red fluorescent protein (RFP), which was co-expressed with IFITM1, in transduced 5H cells. **(E)** *IFITM1* mRNA expression levels in mock-infected and MV-infected hTERT, 5H and 5H-IFITM1 cells at 24hpi. Data shown are relative to housekeeping gene GAPDH and normalized to uninfected control cells (n=3). **(F)** Immunoblots confirming the overexpression of IFITM1 in transduced 5H cells. GAPDH is used as a loading control. Data is expressed as mean ± SEM. All results shown are representative of three independent experiments. (unpaired *t*-test, *p<0.05, **p<0.01, ***p<0.001). NS, not significant.

Figure 7 IFITM1 has anti-viral properties and partly restricts MV infection. (A) Cell viability of 5H cells and IFITM1-overexpressing 5H cells was assessed by trypan blue exclusion at 24 and 48 hours post infection with MV-NSe (MOI of 1.0). Data is

expressed as a percentage of cell killing by MV relative to mock-infected control cells (*n*=3). **(B)** MV-N gene expression measured by RT-qPCR at 24hpi. Results shown are relative to GAPDH and normalized to mock-infected control cells (*n*=3). **(C)** Representative fluorescence microscopy images of MV-GFP infected non-transduced and 5H-IFITM1 cells. Scale bar, 300μm. **(D)** IFITM1 mRNA expression was measured by RT-qPCR at 24hpi. Results shown are relative to GAPDH and normalized to mock-infected control cells (*n*=3). All data is expressed as mean ± SEM (unpaired *t*-test, *p<0.05, **p<0.01, ***p<0.001). MV= measles virus, UI= uninfected, NS= not significant.

Using a well-characterized, step-wise cellular transformation model to determine the mechanism of selectivity of oncolytic measles virus (MV), Aref and colleagues demonstrated the key contribution of the type-1 interferon pathway in resistance to MV-mediated oncolysis. They also showed that *IFITM1* acts as a restriction factor for oncolytic MV strains at early stages of infection.

Figure 1 Model of stepwise transformation of human bone marrow-derived mesenchymal stromal cells (MSCs)

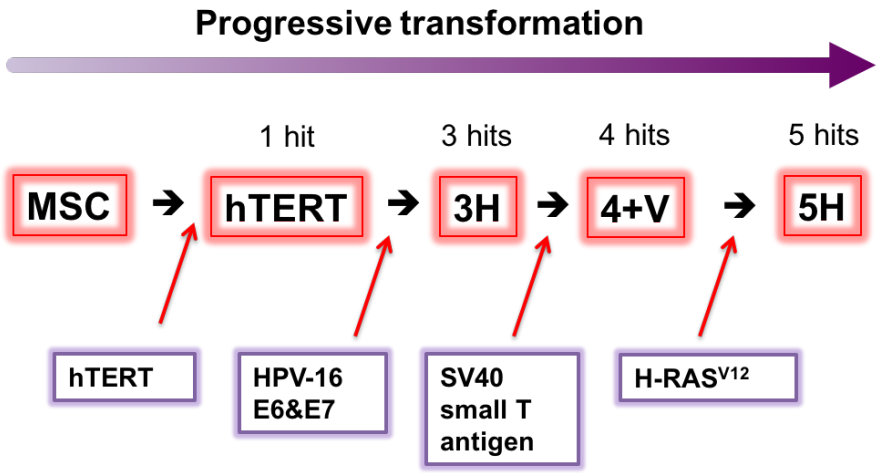

Schematic diagram of MSC stepwise transformation (adapted from Funes *et al.* 2007), MSCs were named according to the number of oncogenes inserted by retroviral transduction. hTERT encodes the catalytic subunit of human telomerase and confers the cells extended lifespan *in vitro.* Human papilloma virus (HPV-16) E6 and E7 genes abrogate the functions of *p53* and *pRb* tumour suppressors, respectively. SV40 small T antigen leads to the stabilization of *c-Myc* by inactivating protein phosphatase 2A. Finally, the insertion of an oncogenic allele of *Ras (H-Ras*^{V12}) provides the acquisition of a constitutive mitogenic signal.

Figure 2 Susceptibility to MV-mediated oncolysis is positively correlated with progressive transformation of MSCs

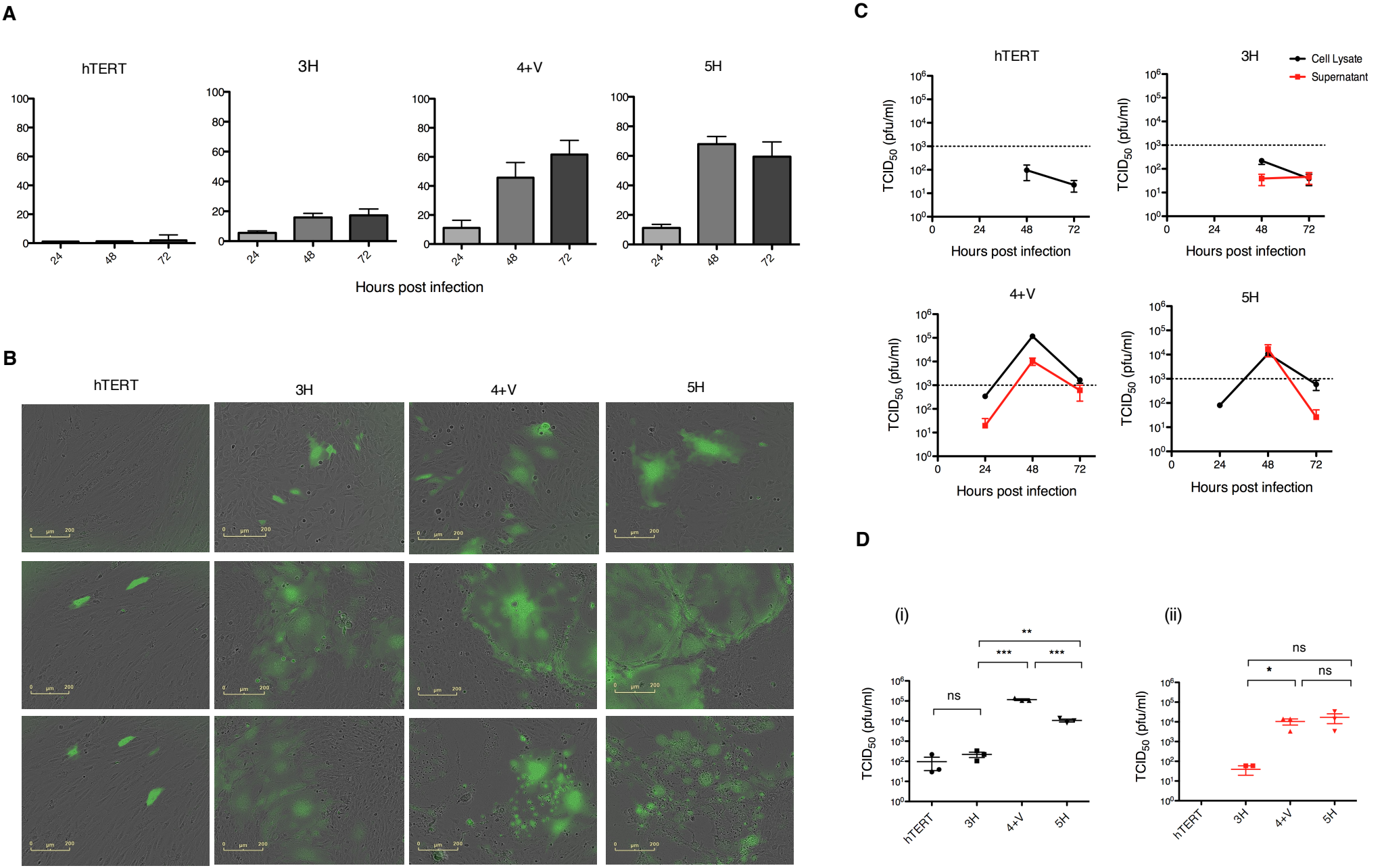

Figure 3 Differential production of type 1 IFN by MSCs in response to oncolytic MV

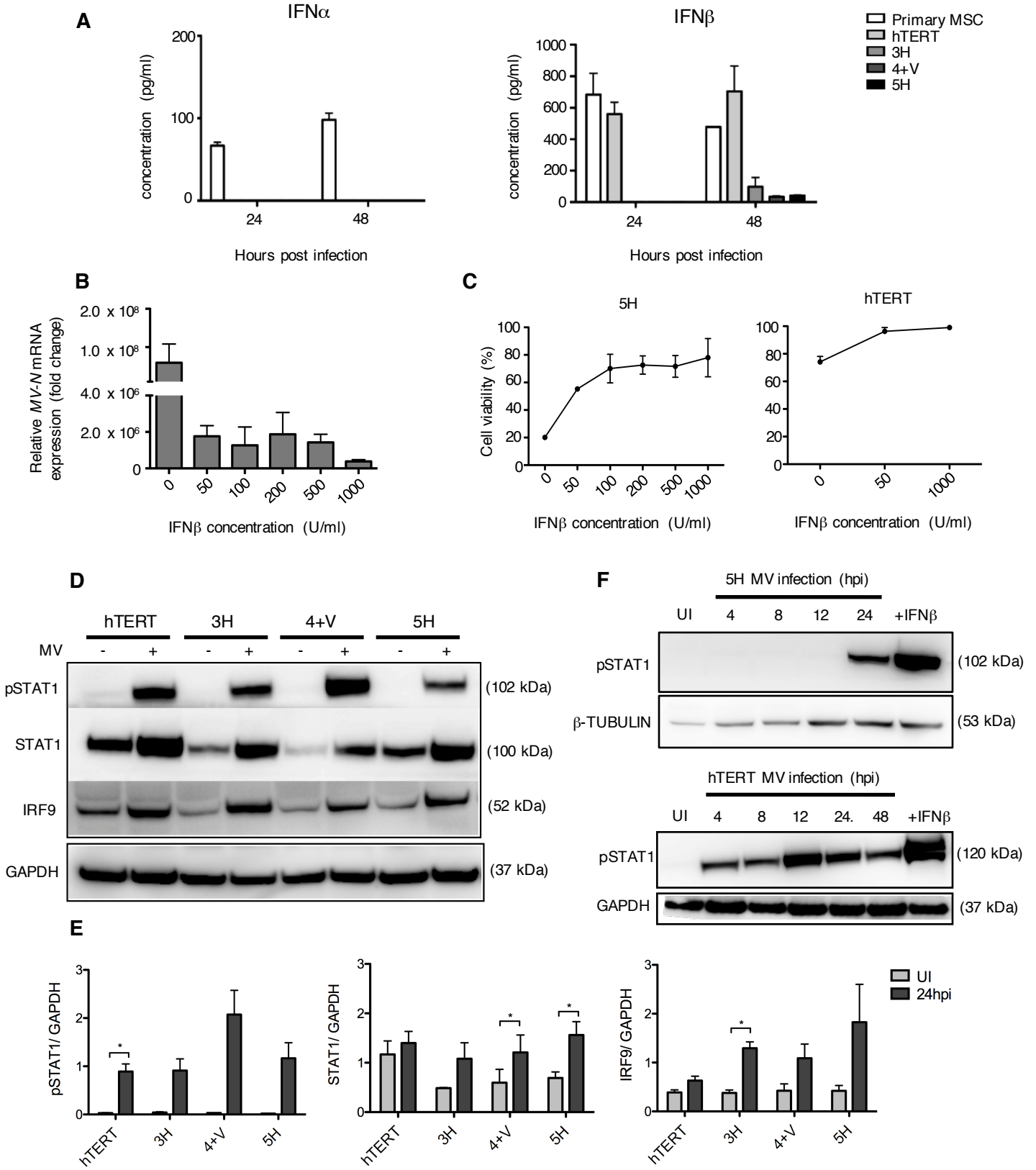

(A) IFNα and IFNβ production levels as assessed by ELISA using tissue culture supernatants collected from all MSCs, including primary patient-derived MSCS, at 24hpi and 48hpi. Data is expressed as mean ± S.E.M of two independent experiments (*n*=2) with samples measured in duplicates. **(B)** *MV-N* mRNA expression levels as assessed by qRT-PCR for 5H cells pre-treated with different concentrations of exogenous IFNβ for 16 hours prior to MV infection. Data shown are relative to housekeeping gene *GAPDH* and normalized to uninfected control cells. Data is expressed as mean ± S.E.M (*n*=3) **(C)** Cell viability of 5H cells following pre-treatment with IFNβ and MV infection was assessed by trypan blue exclusion at 30hpi. hTERT cells were used as a control. Results are reported as a percentage of cell viability relative to uninfected control cells. Data is expressed as mean ± S.E.M (*n*=3). **(D)** Immunoblotting of total STAT1, phosphorylated STAT1 (pSTAT1) and IRF9 using cell lysate of uninfected and MV-infected MSCs collected at 24hpi. Beta-tubulin or GAPDH were used as loading controls (*n*=3) **(E)** Densitometry analysis of blot in (D) performed by ImageJ. **(F)** Immunoblot analysis of pSTAT1 during the time course of MV infection in 5H cells and hTERT cells using cell lysates collected at the indicated timepoints. Cells stimulated with IFNβ (1000U/ml) for one hour were used as a positive control. Beta-tubulin and GAPDH expression were used as loading controls as indicated.

Figure 4 RNA sequencing reveals differential baseline gene expression in MV-resistant and MV-susceptible MSCs

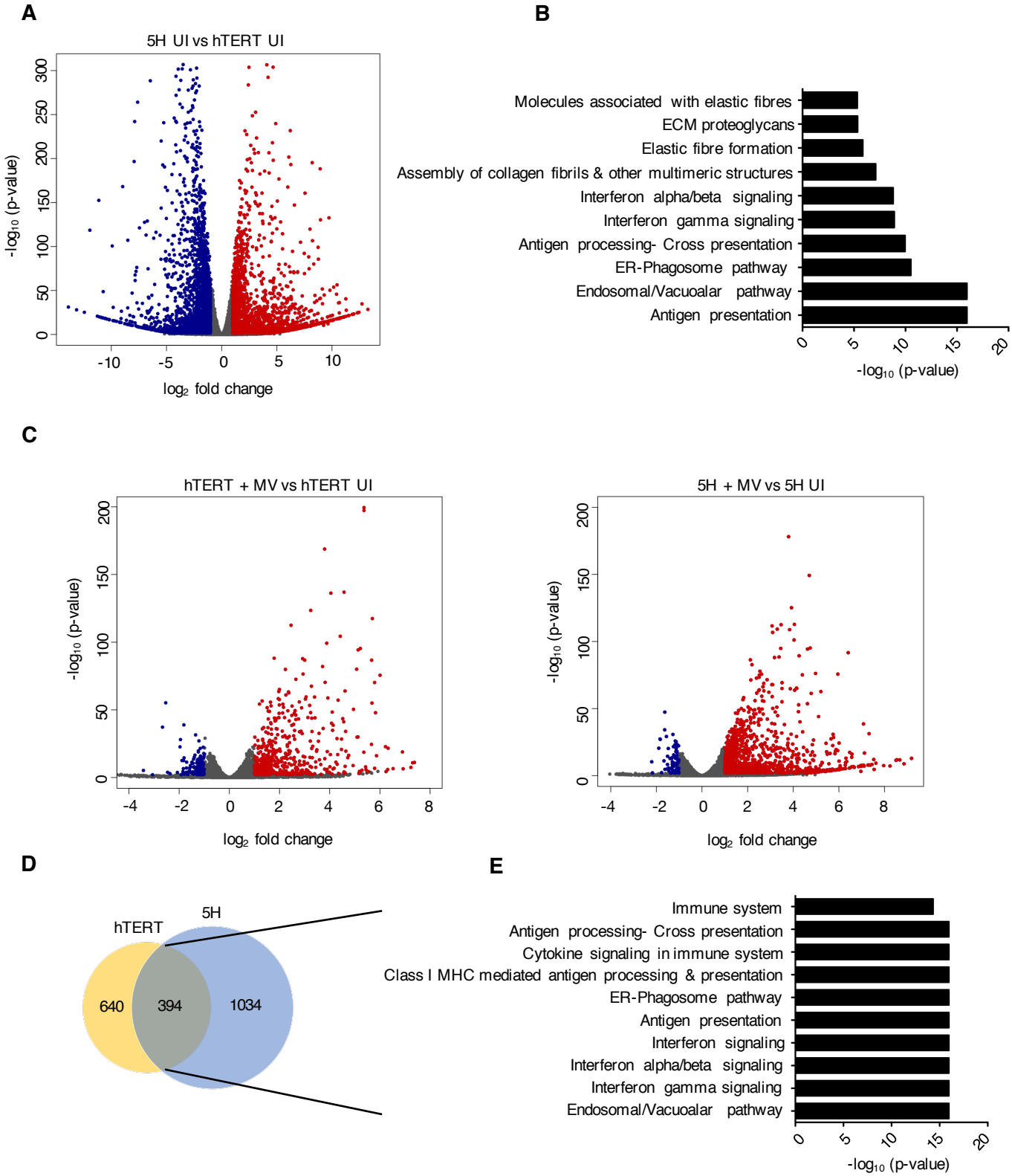

RNA-seq was performed on total RNA was extracted from uninfected and MV-infected hTERT and 5H cells at 24hpi (n=3) **(A)** Volcano plot of differentially expressed genes (DEGs) in 5H cells compared to hTERT cells at baseline levels. Cut-off criteria for DEGs are absolute $\log_2$ fold change>1 and $p_{adjusted}$ value <0.05. The y-axis displays the $\log_{10}$ p-value for each gene, while the x-axis displays the $\log_2$ fold change for that gene relative to hTERT. Red dots indicate up-regulated genes, green dots indicate down-regulated genes and grey dots indicate non-significant relative to hTERT. **(B)** Genes down-regulated (more than 3-fold down-regulation, p-value <0.05) in 5H compared to hTERT cells were selected and analysed using the functional annotation tool in REACTOME. The top 12 enriched pathways (p value<0.001) are shown. **(C)** Volcano plots depicting DEGs after infection of (i) hTERT cells and (ii) 5H cells (compared to mock-infected control cells). **(D)** Venn diagram illustrating the overlap of genes found to be up-regulated in response to MV infection in both hTERT and 5H cells (absolute $\log_2$ FC>1, $p_{adjusted}$ value<0.05) **(E)** REACTOME pathway enrichment analysis of the 394 up-regulated genes. The top ten pathways are represented in the bar plot (p value<0.001).

Figure 5 Genes involved in the type 1 IFN signalling pathway are repressed in 5H compared to hTERT cells and induced by MV infection

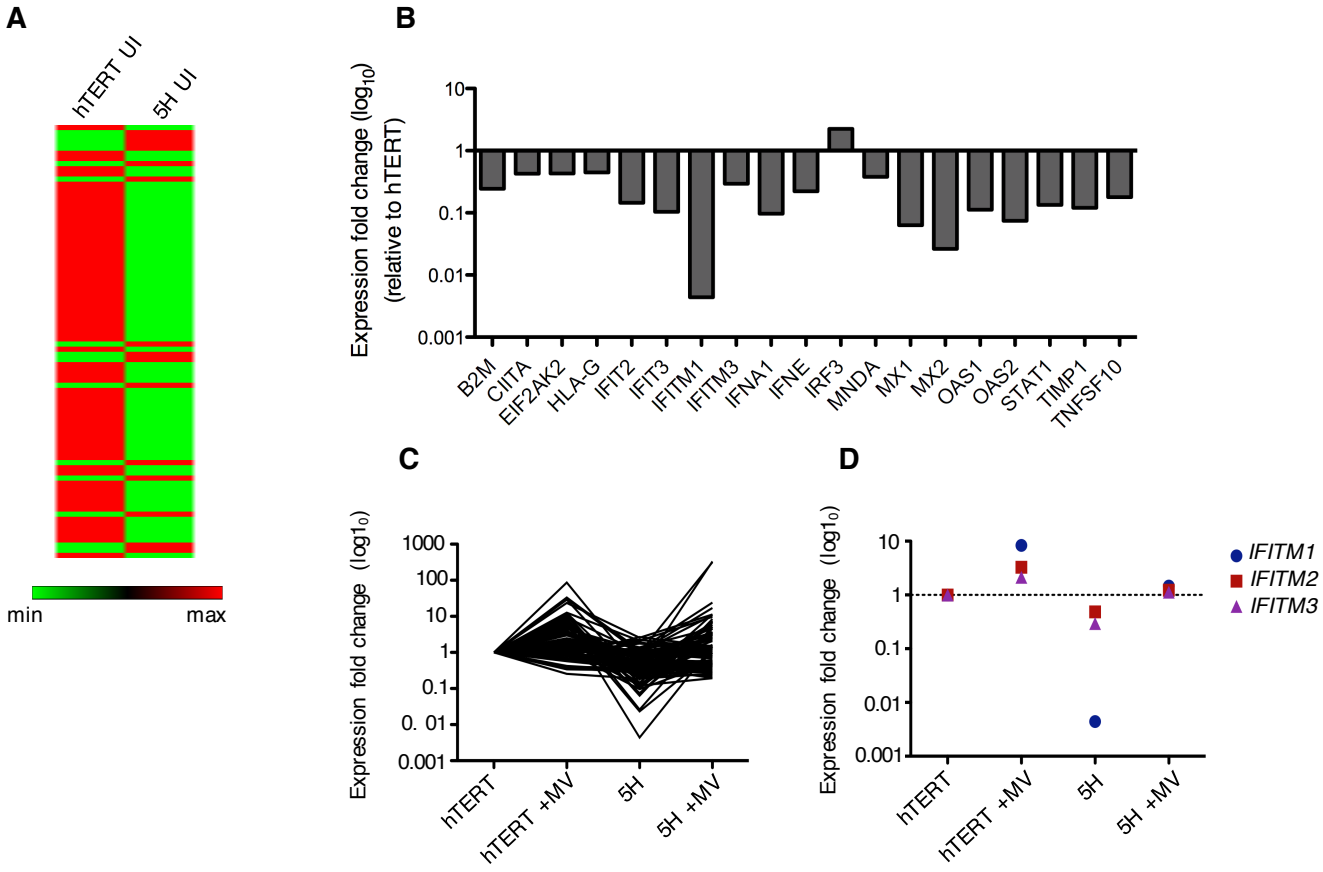

Gene expression of 84 genes was validated by a custom type 1 IFN RT^2 Profiler PCR array. (n=3) **(A)** Heat map representation of array genes in uninfected hTERT and 5H cells. Green represents low expression level, and red represents high expression levels. **(B)** Gene expression profile showing differentially expressed genes in 5H compared to hTERT (absolute $\log_2$FC>1 and $p<0.05$). Gene names are shown on the x-axis. Data is expressed as mean ± SEM. **(C)** Fold change in gene expression of the 84 analysed genes at basal levels and upon induction by MV infection. **(D)** Differential expression of IFITM genes (IFITM1, IFITM2 and IFITM3) before and after MV infection of hTERT and 5H cells. For IFITM1, hTERT vs. 5H *p=0.0338.

Figure 6 IFITM1 expression is correlated with progressive MSC transformation

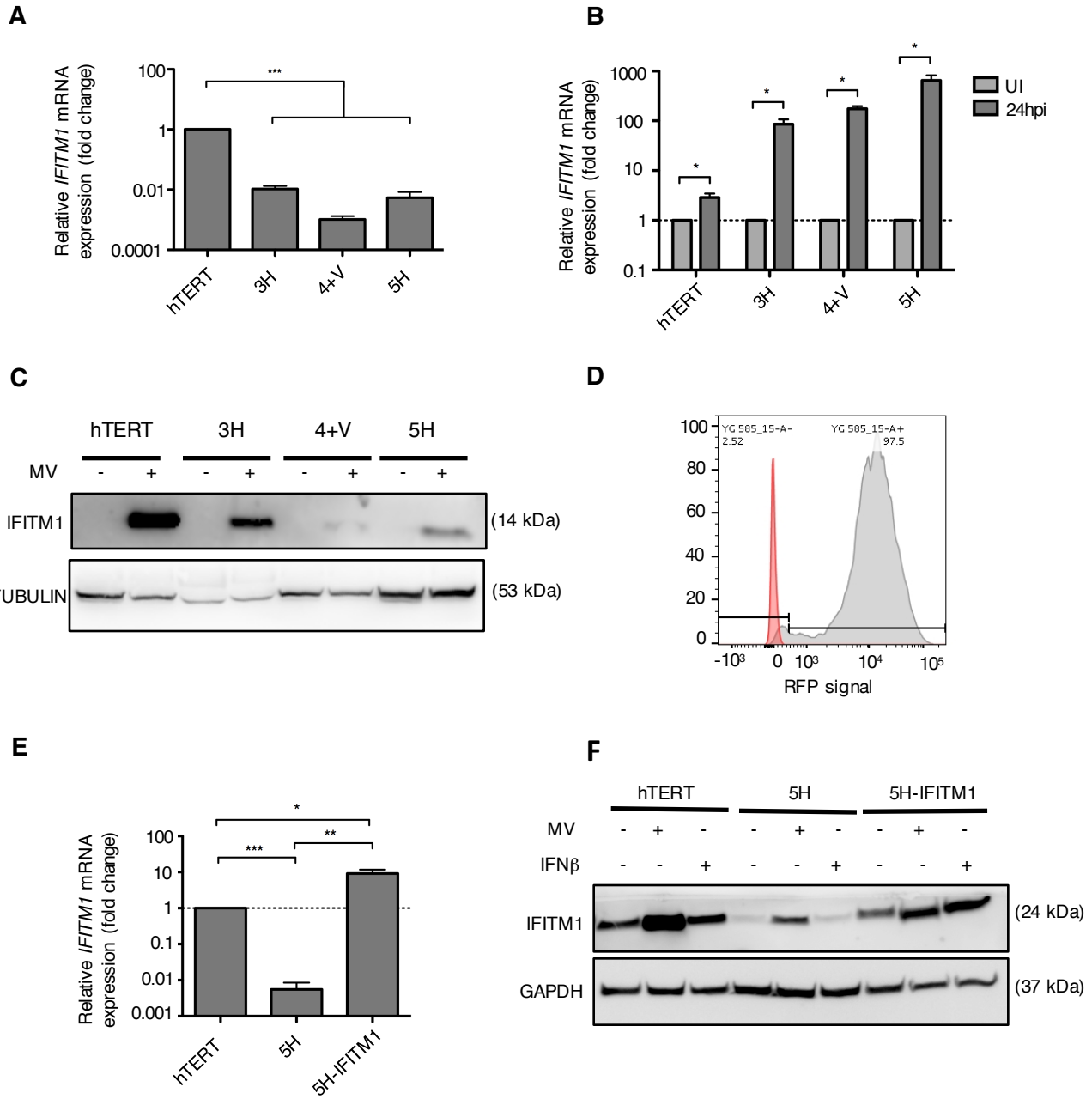

(A) *IFITM1* mRNA expression in all MSCs as assessed by qRT-PCR. Data shown are relative to housekeeping gene *GAPDH* and normalized to hTERT cells. (*n*=3) **(B)** *IFITM1* mRNA expression measured by qRT-PCR at 24hpi of all MSCs. Data shown are relative to housekeeping gene *GAPDH* and normalized to uninfected control cells. (*n*=3) **(C)** Immunoblot showing IFITM1 protein expression at 24hpi in uninfected and MV-infected MSCs. Beta-tubulin is used as a loading control. **(D)** Histograms of FACS analysis of the expression levels of red fluorescent protein (RFP), which was co-expressed with IFITM1, in transduced 5H cells. **(E)** *IFITM1* mRNA expression levels in mock-infected and MV-infected hTERT, 5H and 5H-IFITM1 cells at 24hpi. Data shown are relative to housekeeping gene GAPDH and normalized to uninfected control cells. (*n*=3). **(F)** Immunoblots confirming the overexpression of IFITM1 in transduced 5H cells. GAPDH is used as a loading control. Data is expressed as mean ± SEM. All results shown are representative of three independent experiments. (unpaired *t*-test, *p<0.05, **p<0.01, ***p<0.001). NS, not significant.

Figure 7 IFITM1 has anti-viral properties and partly restricts MV infection

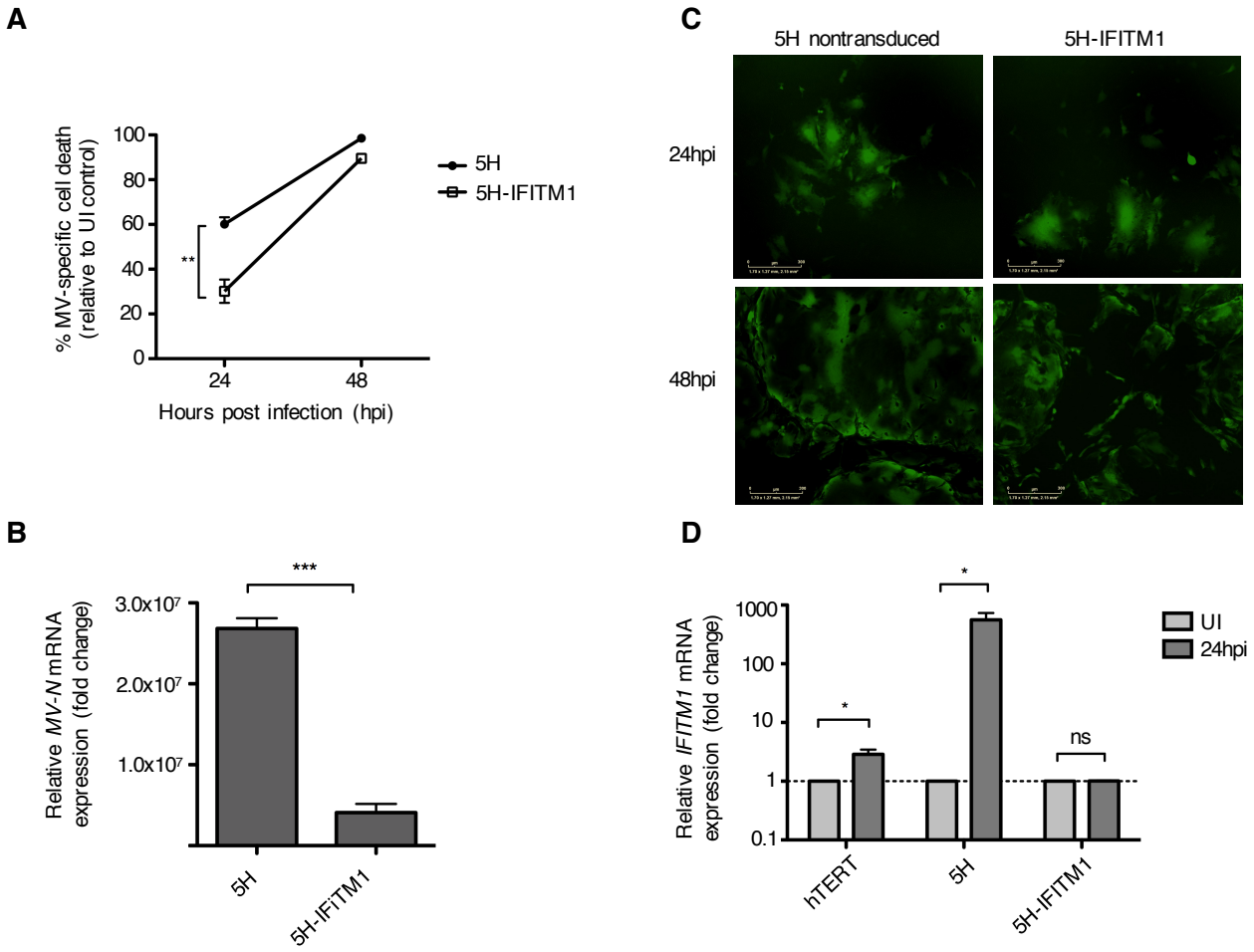

(A) Cell viability of 5H cells and IFITM1-overexpressing 5H cells was assessed by trypan blue exclusion at 24 and 48 hours post infection with MV-NSe (MOI of 1.0). Data is expressed as a percentage of cell killing by MV relative to mock-infected control cells (*n*=3) **(B)** MV-N gene expression measured by RT-qPCR at 24hpi. Results shown are relative to GAPDH and normalized to mock-infected control cells (*n*=3). **(C)** Representative fluorescence microscopy images of MV-GFP infected non-transduced and 5H-IFITM1 cells. Scale bar, 300µm. **(D)** IFITM1 mRNA expression was measured by RT-qPCR at 24hpi. Results shown are relative to GAPDH and normalized to mock-infected control cells (*n*=3). All data is expressed as mean ± SEM (unpaired *t*-test, *p<0.05, **p<0.01, ***p<0.001). MV= measles virus, UI= uninfected, NS= not significant.